INTERNATIONAL ATOMIC ENERGY AGENCY
UNITED NATIONS EDUCATIONAL, SCIENTIFIC AND CULTURAL ORGANIZATION
INTERNATIONAL CENTRE FOR THEORETICAL PHYSICS
I.C.T.P., P.O. BOX 586, 34100 TRIESTE, ITALY, CABLE: CENTRATOM TRIESTE

SMR.703 - 14

WORKING PARTY ON
MECHANICAL PROPERTIES OF INTERFACES

23 AUGUST - 3 SEPTEMBER 1993

"Interfaces: Structure and Properties" (Part II)

"Structure-Energy Correlation for Grain Boundaries in Metals"

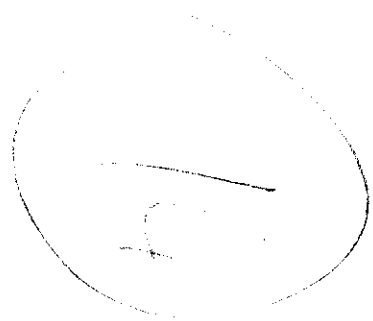

Dieter WOLF
Materials Science Division
Argonne National Laboratory
9700 S. Cass. Avenue
Building 233
Argonne, IL 60439
U.S.A.

These are preliminary lecture notes, intended only for distribution to participants.

Structure and Energy of Grain Boundaries in Metals

K.L. Merkle and D. Wolf

Introduction

The investigation of structure-property correlations is a rather complex endeavor not only because interfacial systems are intrinsically inhomogeneous, with chemical composition and physical properties differing from the surrounding bulk material, but also since three different aspects of the geometrical structure are involved — namely the macroscopic, microscopic, and atomic structures. As outlined in the Guest Editors' introduction, in addition to the choice of the materials which form the interface, five macroscopic and three microscopic degrees of freedom (DOFs) are needed to characterize a single bicrystalline interface.[1] The importance of the atomic structure at the interface as well as the local interfacial chemistry, extrinsic (i.e., impurity segregation) or intrinsic (for example, via interfacial reactions or space-charge phenomena), greatly add to the task's complexity.

Grain boundaries (GBs) in pure metals represent ideal model systems for investigating the strictly geometrical aspects of structure-property correlations for the following three reasons. First, the complexity due to the myriad of possible choices of materials combinations forming the interface is avoided, enabling a focus on the different roles of the three distinct geometrical aspects of the structure. Second, because GBs are bulk interfaces, dimensional interface parameters (such as the modulation wavelength in strained-layer superlattices, or the thickness of epitaxial layers) do not enter into the problem. Finally, the GB energy is thought to play a central role in various GB properties, such as impurity segregation, GB mobility and fracture, GB diffusion and cavitation, to name a few. A better understanding of the correlation between the structure and energy of GBs, therefore, promises to offer insights into more complex structure-property correlations, as well. Also, it represents a base line against which the effects of interfacial chemistry can be probed.

Despite various controlled bicrystal experiments performed to date, a systematic experimental exploration of the misorientation phase space associated with the five macroscopic and three microscopic DOFs of a single flat GB has not been performed. Because of the relative ease with which the macroscopic DOFs can be manipulated in the computer, an approach using the complementary capabilities of atomic-level computer simulation and experiment seems to be particularly promising. However, while a comparison between experiments and modeling results in crucial test cases is absolutely essential, the main strength of such simulations lies in their ability to provide atomic-level insights into structure-property correlations. In this spirit we describe the combination of high-resolution electron-microscopy (HREM) observations of the structure of grain boundaries with atomistic computer simulations to investigate the structure and energy of GBs in fcc metals.

In correspondence with the three types of structure-energy correlations to be considered in the following text, three

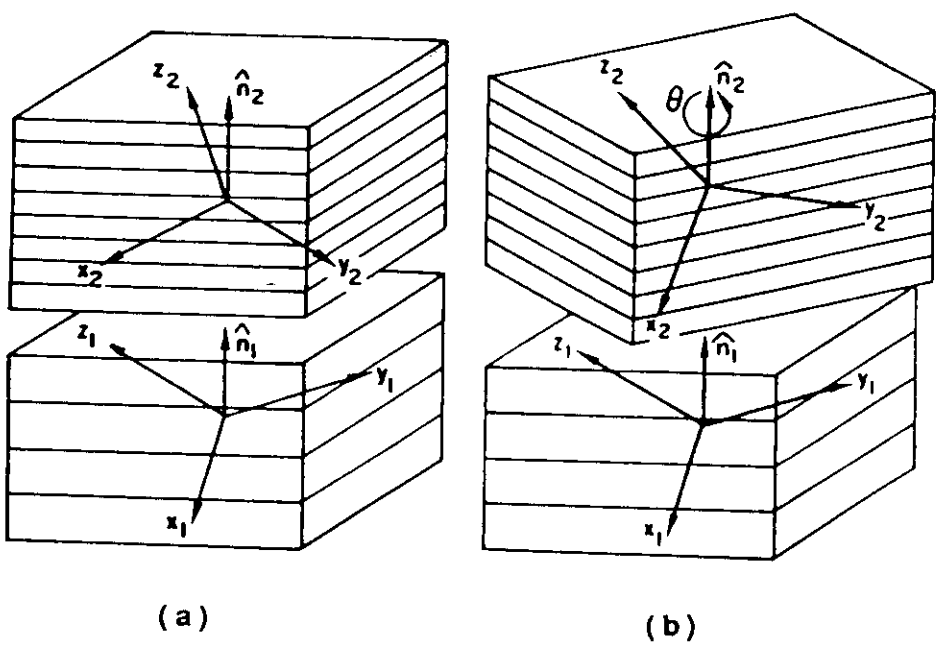

Figure 1. Creation of an "asymmetrical twist" (or general) GB by a twist rotation of an asymmetrical combination of lattice planes about the common GB-plane normal. Two asymmetrical tilt configurations (ATGBs), with identical unit-cell dimensions but inverted stacking sequences, are obtained for θ = 0° and 180°/m (sketched in 1a). (Here m characterizes a possible rotation symmetry (for m > 1) in the planar unit cell of the GB.) For some arbitrary twist angle, θ, an asymmetrical twist GB is obtained (right).[5]

kinds of combined HREM-simulation studies will be highlighted. First, concerning the correlation with the five macroscopic DOFs, the HREM identification of planar facets illustrates the dominating role of the densest planes in the crystal, in agreement with the simulation of GB energies. Second, among the three microscopic DOFs the volume expansion usually observed at metallic GBs is most directly related to the GB energy; this expansion can be determined via both simulation and HREM experiments. Finally, the atomic structures observed in HREM experiments typically consist of well-matched regions separated by highly localized areas of misfit. The origin of this tendency to maintain perfect-crystal coordination at the interface is elucidated by extensive simulations showing a direct correlation between the number of broken nearest-neighbor bonds per unit area of the GB and its energy.

Grain-Boundary Geometry

A systematic investigation of structure-property correlations for GBs should, from the outset, be based on a thorough understanding of the basic geometry of bicrystalline interfaces. As is well known, five macroscopic and three microscopic DOFs must be specified to characterize a general GB.[1] (If the GB is mobile, a sixth DOF is needed to characterize the position of the GB plane.) While the three microscopic DOFs are usually represented by a vector, **T**, associated with rigid-body translations of the two halves relative to one another, parallel (T_x,T_y) and perpendicular (T_z) to the GB plane, the five macroscopic DOFs fully determine the type of the GB, i.e., whether it is of a pure tilt, twist or mixed (general) type, whether it is symmetrical or asymmetrical, or whether it is of a low- or high-angle type.

Within the framework of the coincident-site lattice (CSL) description of GBs[2], three out of the five macroscopic DOFs are identified with the CSL misorientation, and only the remaining two DOFs are assigned to the GB plane. (The inverse density of CSL sites, Σ, is usually added as a sixth parameter.) Because of the consequent focus on the misorientation between the two grains, rather than the plane of the defect, the CSL-based terminology is not usually applied to interfaces other than grain boundaries, thus rendering a comparison of properties of different interfacial systems virtually impossible. A more useful choice of the five macroscopic DOFs, applicable to both commensurate and incommensurate interfacial systems, focuses on the importance of the interface plane by assigning to it *four* of the five DOFs as follows (see Figure 1):[3]

$$\{\text{DOFs}\} = \{\hat{n}_1,\hat{n}_2,\theta\} \qquad (1)$$

Here the unit vectors $\hat{n}_1$ and $\hat{n}_2$ (i.e., four DOFs) represent the GB-plane normal, however, they are rotated respectively into the principal coordinate systems of semi-crystals 1 and 2, forming the bicrystal. For example, $\hat{n}_1$ and $\hat{n}_2$ might be the normals of (100) and (115) planes, respectively. By definition, the angle θ (one DOF) describes a twist rotation (i.e., about the GB-plane normal; see Figure 1), because any other rotation would change $\hat{n}_1$ and $\hat{n}_2$.

The twist component of a general boundary described by Eq. 1 is therefore governed by θ and by the GB-plane normal, while its tilt component, governed by the condition that $\hat{n}_T \perp \hat{n}_1,\hat{n}_2$, is given by[4]

$$\hat{n}_T = [\hat{n}_1 \times \hat{n}_2]/\sin\Psi, \qquad (2)$$

$$\sin\Psi = (|\hat{n}_1 \times \hat{n}_2|), \qquad (3)$$

where $\hat{n}_T$ is a unit vector defining the orientation of the tilt axis and Ψ denotes the tilt angle.

Equations 2 and 3 illustrate that the tilt component of a general boundary, defining $\theta = 0°$, is fully determined by the normals $\hat{n}_1$ and $\hat{n}_2$; i.e., by the GB plane (see Figure 1a). $\theta = 0°$ thus characterizes a GB with the smallest planar unit cell of all GBs formed by the same combination of planes; any non-zero value of θ (see Figure 1b) increases the planar unit-cell area. $\theta = 0°$ thus characterizes an asymmetrical tilt boundary (ATGB), while for an arbitrary value of θ, a general boundary is obtained.

It is important to recognize that for the same combination of lattice planes forming the GB, a second ATGB configuration is found at $\theta = 180°/m$. (Here m characterizes a possible rotation symmetry (for $m > 1$) in the planar unit cell of the GB.) Two ATGB configurations exist because in crystal lattices with inversion symmetry, a twist rotation by $\theta = 180°/m$ leads to an inversion of the stacking sequence of the lattice planes, say in the top half of Figure 1a with respect to the bottom half.[3,4] In the fcc lattice, there are two exceptions: Because of the ...|AB|AB|... stacking, the inversion of the (100) and (110) planes by a $180°/m$ twist rotation about ⟨100⟩ or ⟨110⟩, respectively, can be undone simply by a rigid-body translation parallel to the plane, thus restoring the perfect crystal configuration. Therefore, in asymmetrical GBs with a (100) or (110) plane on one side of the interface, the two ATGBs are identical. To better visualize the effect of a twist rotation by $180°/m$, one may simply think of its net effect as the turning upside down of one of the two semi-crystals in Figure 1a.

Since (1) the inversion of the stacking sequence preserves the planar unit-cell dimensions of the ATGB at $\theta = 0°$, and (2) an θ twist deviation from $\theta = 0°$ and $\theta = 180°/m$ results in an increase of the planar unit cell of the GB, the two ATGB configurations are unique geometrically

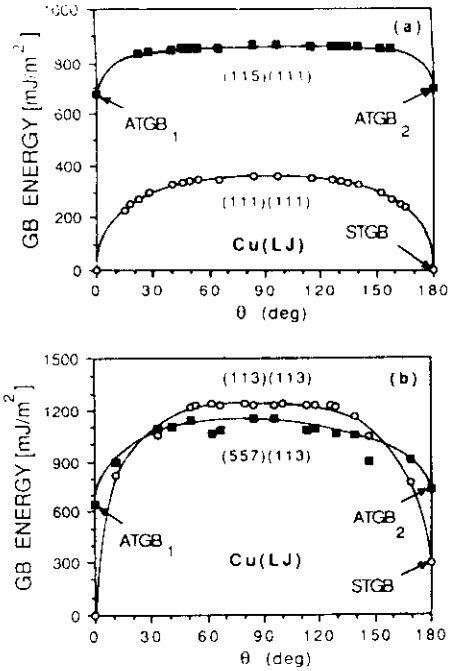

Figure 2. Energies (in mJ/m²) of symmetrical and asymmetrical twist boundaries simulated by means of the LJ potential. The ATGB and STGB configurations at the endpoints, with the smallest planar unit cells, are indicated. Because of the three-fold symmetry axis in the planar unit cells, in 2a the usual misorientation angle, θ_{CSL} was replaced by $\theta = 3\sigma_{CSL}$, thus scaling all angles to 180°. The (111) twin configuration, with an unrealistically low energy of 2 mJ/m² for this and the EAM potential, is thus shifted from $\theta_{CSL} = 60°$ to $\theta = 180°$, as required by Eq. 4. The lines represent least-squares fits of the extended Read-Shockley Eq. 4 to the simulation data.[10]

Figure 3. Transmission electron micrograph of $(1\bar{1}0)$ tilt GB in Au. Coexistence of extended planar symmetric facets (S) with a number of asymmetric facets is evident. Facets labeled D, near (111)(115), are dissociated into coherent and incoherent twin boundaries (see HREM inset).

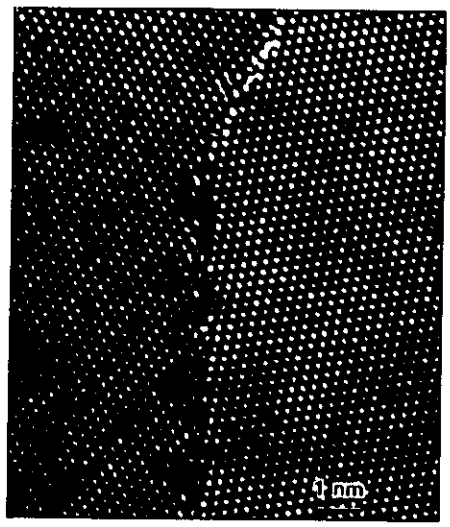

Figure 4. HREM micrograph of $(1\bar{1}0)$ tilt GB in Au, showing a short symmetric (221) facet near the top of the figure and an asymmetric (557)(771) facet with the same misorientation [$\Psi \approx 39°$ ($\Sigma 9$)]. White spots represent atomic columns.

in that they have identical planar unit-cell dimensions with an area that is the smallest of all GBs formed by the same combination of lattice planes. As illustrated in the next section, this unique geometry translates into a particularly low energy, giving rise to "special" properties of these two configurations at the endpoints of the twist-misorientation range.

Symmetrical GBs are obviously characterized by the condition that $\hat{n}_2 = \pm\hat{n}_1$ in Eq. (1), thus reducing the number of DOFs from five to only three (see also Figure 1). $\theta = 0°$ now corresponds to the perfect crystal while, for some arbitrary value of θ, a pure twist boundary (with three DOFs) is obtained. As in the asymmetrical case, a twist rotation by $\theta = 180°/m$ inverts the stacking sequence on one side of the GB plane with respect to the other while preserving the perfect-crystal planar unit-cell dimensions.[3] Consequently, the symmetrical tilt boundary (STGB) that is obtained is fully determined by only the two DOFs associated with the GB-plane (because θ is fixed at $180°/m$). Its atomic structure is characterized by the familiar twinning of the lattice planes at the interface, a feature common to all STGBs.[3,4]

As in the asymmetrical case, for any twist deviation from $\theta = 0°$ and $\theta = 180°/m$ the planar unit-cell area also increases in the symmetrical case. The STGB and perfect-crystal configurations on a given plane are therefore unique in that they share identical planar unit-cell dimensions, with an area that is the smallest possible for any planar defect on that plane. As illustrated later, this unique geometry of the pure tilt configuration gives rise to a deep energy cusp at $\theta = 180°/m$, and therefore to "special" properties of STGBs by comparison with twist boundaries. Also, since both STGBs and free surfaces are characterized by only the two DOFs associated with the interface plane, the properties of these two simplest types of all planar defects can be compared directly. However, because free surfaces lack the three translational DOFs of GBs, the related three-dimensional (3d) structure-energy plots show some interesting differences (see below).

The above choice of the five DOFs has essentially three advantages over the CSL-based definition of the macroscopic DOFs. First, the resemblance of a general boundary (with five DOFs) with a pure twist boundary (with three DOFs) becomes apparent (see Figure 1b) in that (1) the beginning and endpoints of the twist rotation, at $\theta = 0°$ and $\theta = 180°/m$, represent pure tilt boundaries (see Figure 1a), with the smallest possible planar unit cells, and (2) both may be viewed as having been generated by a twist rotation about the GB-plane normal. The term asymmetrical twist boundary therefore appears to reflect the geometry of a general boundary more succinctly;[5] its tilt and twist components are apparent in that any asymmetry in the GB plane automatically implies the existence of a tilt component (see Eqs. 2 and 3). Second, incorporated naturally in the description is that—from a purely geometrical point of view—tilt boundaries represent a special subset of symmetrical or asymmetrical twist boundaries, thus greatly simplifying the exploration of the five-parameter misorientation phase space associated with the macroscopic DOFs (see below). Finally, the above choice of macroscopic DOFs is not limited to the description of commensurate systems and is, in fact, rather commonly applied to coherent or incoherent dissimilar-material interfaces, thus enabling a more direct comparison of the different basic types of interface systems defined in the Editors' Introduction.

Correlation Between Macroscopic Degrees of Freedom and GB Energy

Using the previously developed terminology, we can now address the first of the three aspects of the structure-energy correlation, namely the variation of the

GB energy in the five-parameter misorientation phase space defined in Eq. 1.

Energies of Symmetrical and Asymmetrical Grain Boundaries

An iterative energy-minimization algorithm ("lattice statics") was used to compute the fully relaxed zero-temperature atomic structures and energies of GBs. By computing the forces that the two halves of a bicrystal exert on each-other, translations parallel to the GB plane (T_x, T_y) are allowed while the atoms relax. Also, to enable the GB to expand or contract (related to T_z), the unit-cell dimension in the direction of the GB normal is allowed to increase or decrease in response to the internal pressure. By starting from a variety of initial rigid-body translational configurations, the GB energy may thus be minimized with respect to both the atomic positions and the three microscopic DOFs.

Figures 2a and 2b show typical variations of the GB energy, $E^{GB}(\theta)$, for two different symmetrical and asymmetrical combinations of lattice planes. While these results were obtained using a Lennard-Jones (LJ) pair potential fitted for Cu, a semi-empirical many-body potential of the embedded-atom-method (EAM) type fitted for Au[6] gives qualitatively identical results; throughout, therefore, results from both types of potentials will be used.

In all four cases, the tilt configurations at the endpoints give rise to pronounced energy cusps, separated by more or less flat plateau regions in which the energy is practically independent of θ. The physical origin of these cusps lies in the especially small planar unit cells of STGBs and ATGBs discussed previously, which enable a better local interlocking of the atom positions across the GB than in twist boundaries, thus permitting their energy to be minimized more effectively.[3] This explains the preponderance of tilt boundaries (symmetrical and asymmetrical) in recent "rotating-sphere-on-a-plate" experiments in which the GB planes and types were identified, with only a small fraction representing twist GBs.[7]

Replacing one of the two sets of symmetrical planes, thus creating asymmetrical boundaries, has a profound effect on the GB energy in the two cases (compare Figures 2a and 2b). While the replacement of the densest (111) planes in the fcc lattice (see Table I) by less dense (115) planes leads to a significant increase in the GB energy over the entire misorientation range (see Figure 2a), the energy in the plateau region actually decreases when (557) planes are substituted for the fourth-densest (113) planes (see Figure 2b). Interestingly, however, the (113) STGB nevertheless has a lower energy than the (557)(113) ATGB configuration at $\theta = 180°$ (see also Figure 10). This indicates an important role played by the particular lattice planes forming the GB. It also suggests that some asymmetrical GB-plane orientations may have a lower GB energy than related symmetrical ones, although the asymmetry may affect tilt and twist boundaries in different ways. Also notice, however, that despite the sharp increase in energy on substituting (115) planes for (111) planes, the energies of the (115)(111) boundaries are nevertheless significantly lower than those of the boundaries in Figure 2b with a (113) plane on one or both sides of the interface. This strongly suggests an important role of the densest lattice planes in the energies of not only symmetrical[3,8] but also asymmetrical GBs.[5]

As illustrated by the solid lines in Figures 2a and 2b, a quantitative analysis of the variation of the GB energy per unit area as a function of θ may be based on an empirically extended Read-Shockley equation[9] in which θ is simply replaced by $\sin\theta$, according to[10]

$$E^{GB}(\theta) = E^{GB}(\theta = 0°) + \sin\theta[E_c - E_s ln(\sin\theta)]/b, \quad (0° \le \theta \le 90°), \quad (4)$$

where b is the Burgers vector. The core and strain-field energies per unit length of the GB dislocations, E_c and E_s, (in this case screw dislocations because E^{GB} varies as a function of the twist angle) are regarded as adjustable fitting parameters.[10] An analogous expression can be written for the other half of the misorientation range ($90° \le \theta \le 180°$). Similar expressions also hold for the volume expansion at the GB.[10] Based on the physics of lattice dislocations, Eq. 4 thus permits the θ dependence of the GB energy to be described analytically. The remaining problem in the investigation of the macroscopic structure-energy variation therefore lies in understanding the GB plane's role.

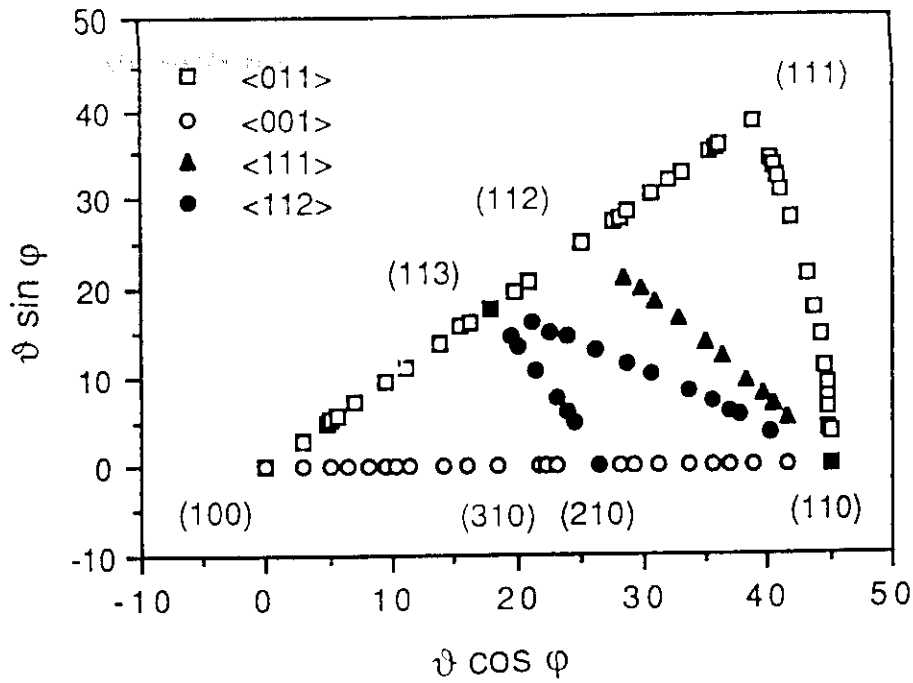

Figure 5. Schematic plot, similar to the stereographic triangle, of the distribution of STGB planes simulated to explore the 2d phase space associated with the GB-plane normal. Orientations perpendicular to ⟨100⟩, ⟨110⟩, ⟨111⟩ and ⟨112⟩ tilt axes are included. δ and φ are the two DOFs associated with the polar and azimuthal angles characterizing the GB-plane normal. δ is in degrees.

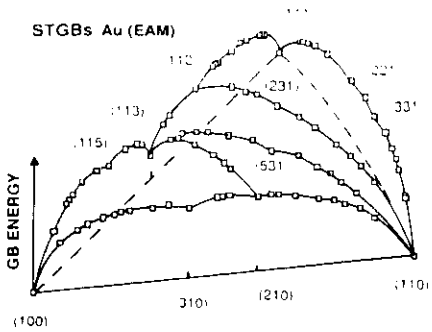

Figure 6. 3d structure-energy plot computed for the EAM potential, illustrating the correlation between the energy and GB-plane normal for STGBs. The base plane is represented by the phase-space triangle defined in Figure 6. A similar plot is obtained for the LJ potential.

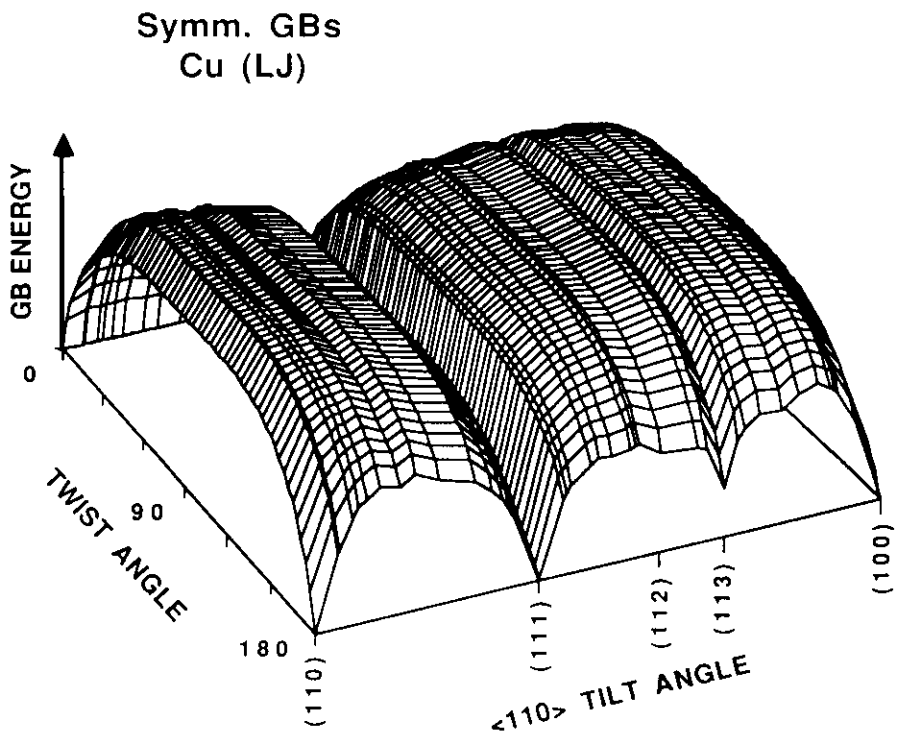

Figure 7. 3d cross section, for GB planes perpendicular to ⟨110⟩, of the 4d structure-energy hypersurface associated with symmetrical GBs in fcc metals. The STGBs are seen for the twist angles of 180°. The figure illustrates that in the 3d misorientation phase space associated with all symmetrical GBs, the symmetrical tilt boundaries represent an infinitely small subset of twist boundaries. Similar plots have also been obtained for GB planes perpendicular to ⟨100⟩, ⟨111⟩ and ⟨112⟩.[14]

Table I: Interplanar spacing, *d(hkl)* (in units of the lattice parameter *a*), for the 11 most widely spaced planes in the fcc lattice. These planes also correspond to the ones with the highest planar density of atoms, (i.e., the smallest planar repeat unit cells).

No.	(hkl)	d(hkl)/a
1	(111)	0.5774
2	(100)	0.5000
3	(110)	0.3535
4	(113)	0.3015
5	(331)	0.2294
6	(210)	0.2236
7	(112)	0.2041
8	(115)	0.1925
9	(513)	0.1690
10	(221)	0.1667
11	(310)	0.1581

HREM Investigation of the GB Plane

From the experimental point of view, the fact that—due to their unique geometry—tilt boundaries are energetically preferred is a very fortunate circumstance because these are the only GBs whose atomic structure is readily accessible by HREM methods. However, for reasons of limited resolution, the observation of atomic columns parallel to the tilt axis is only possible for relatively densely-packed tilt directions. With no twist components, the energy of these boundaries is governed completely by the four DOFs associated with the GB plane (see Eqs. 2 and 3); tilt boundaries thus represent ideal model systems for an experimental investigation of the role of the GB plane. Our basic idea is the following: By forming tilt bicrystals with a well-defined tilt misorientation between the two grains (for example, via a sintering technique[11,12]), in principle the GB plane is free to chose any symmetrical or asymmetrical configuration that is energetically favored. Assuming the GBs observed in such bicrystals to be thermally equilibrated, edge-on HREM characterization of the observed facets and their lengths should reveal the preferred (i.e., lowest-energy) boundary planes.

In one such effort,[13] tilt boundaries in Au with a common ⟨110⟩ tilt axis were manufactured by sintering two thin (110) gold films (which were grown epitaxially on NaCl in a UHV system) together at the appropriate tilt angle Ψ, thus fixing the value of Σ. After removal from the NaCl substrate, columnar grains misoriented by the desired tilt angle were obtained by further annealing. HREM samples were then prepared by ion-beam milling followed by a 225° C anneal. Typically, high-resolution images were taken at a magnification of 700,000 X for several defocus values near optimum defocus, using a H9000 high-resolution electron microscope, operated at 300 kV. HREM images generally depend strongly on thickness and defocus values, and therefore need to be interpreted via image simulation, based on atomic models obtained from simulation. For the HREM images shown below, which were taken close to the optimum focus, atomic columns are quite well represented by the bright spots in the images.

Employing conventional transmission electron microscopy, a typical low-resolution edge-on view of several extended planar facets of tilt GBs in Au with a common (110) axis and tilt angle

of $\Psi \approx 40°$ ($\Sigma 9$) is shown in Figure 3. The spatial resolution in this figure is insufficient to determine which interface is present, since, on an atomic scale, the GB may be roughened, form atomic-scale facets, or it may be dissociated. The latter is, in fact, the case at the facets labeled D in Figure 3, as seen in the HREM inset, which shows dissociation of a (115)(111) facet into a combination of coherent and incoherent twin boundaries. Extensive HREM analysis of several Au bicrystals has shown the presence of a finite number of planar facets, indicating that in each case some GB planes are preferred over others. For each misorientation, symmetric and asymmetric facets are found to coexist, as illustrated in Figure 4. Moreover, in many asymmetric facets, one of the densest lattice planes on one side of the interface is combined with some higher-index plane on the other side.

In an attempt to extract more quantitative information on the GB energy from the combination of such experiments with computer simulations, we recently examined several tilt bicrystals of Au, with different misorientations, in the form of small island grains in a single-crystalline matrix. Comparison of the observed faceting behavior with computed energies illustrates that low GB energy indeed manifests itself in long facets. Moreover, many of the asymmetric facets indeed have lower energies than the corresponding symmetric ones, explaining the observed preponderance of asymmetrical GBs. In addition, the dissociation of (115)(111) facets (see the inset in Figure 3) is found to be energetically favored over the asymmetric straight GB-plane configuration. In other cases the multitude of observed facets of similar lengths could be correlated with rather similar magnitudes of the computed energies.

These examples demonstrate the considerable promise of HREM observations combined with computer simulations in furthering our understanding of the energies of GBs.

Structure-Energy Phase Space for Symmetrical GBs

As previously discussed, STGBs and free surfaces represent the conceptually simplest of all crystalline interface systems because both are equally characterized by only the two macroscopic DOFs associated with the interface plane. Their macroscopic structure-energy correlation, which may thus be displayed in a single 3d plot, should therefore provide additional insight into the importance of the interface plane in the energy.

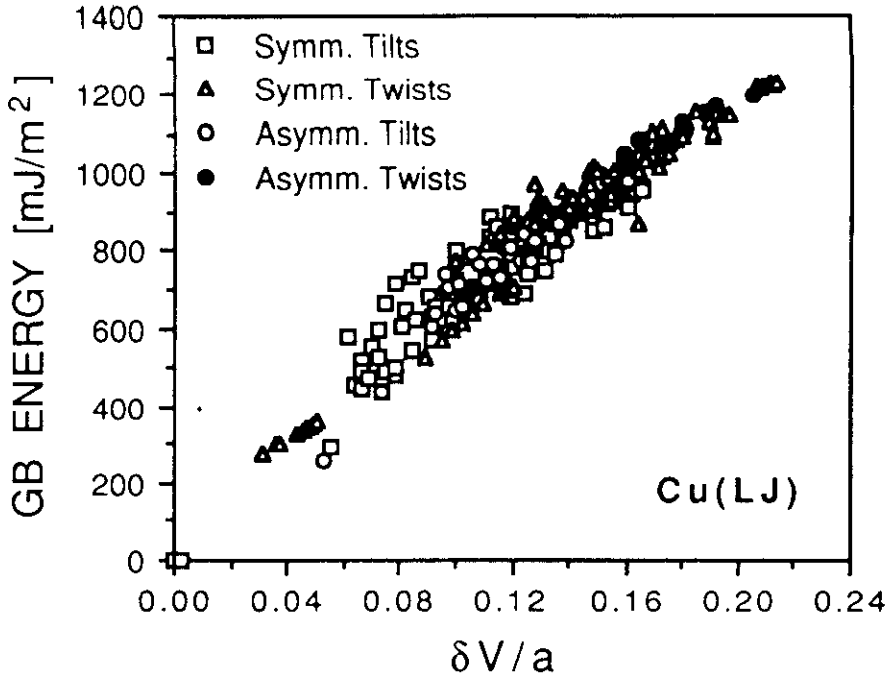

Figure 8. Correlation between the GB energy and volume expansion per unit area, $\delta V/a$ (in units of the lattice parameter a) for symmetrical and asymmetrical tilt and twist GBs (LJ potential; a similar plot is obtained for the EAM potential).[14]

As is well known, in a cubic crystal all orientations, specified by the polar and azimuthal angles δ and ϕ, may be represented by the phase-space triangle sketched in Figure 6—this is similar to the stereographic triangle. Figure 5 shows the distribution of the STGB and free-surface normals considered in our exploration, by means of computer simulation, of this two-parameter $\{\delta,\phi\}$ phase space. The figure also illustrates our motivation for including ⟨111⟩ and ⟨112⟩ tilt or pole axes, in addition to the more popular ⟨110⟩ and ⟨100⟩ orientations: the latter sample only the periphery of the triangle, while the ⟨111⟩ and ⟨112⟩ axes cover its center section.

The overall variation of the energy of STGBs in the 2d phase space is illustrated in Figure 6 (shown here for the EAM potential). A comparison between Figure 6 and the interplanar spacings in Table I demonstrates a close interrelation between the appearance of cusps and a relatively large interplanar spacing, $d(hkl)$, of the planes parallel to the GB. (Note, however, that because of the underlying two-plane (...|AB|AB|...) stacking sequence, the STGB configurations on the (100) and (110) planes are identical to the perfect crystal, thus giving rise to deep cusps.) In Bravais lattices, the planar unit-cell area, $A(hkl)$, of a perfect-crystal (hkl) plane (and hence of the STGB and free surface on that plane) is inversely proportional to $d(hkl)$, since $A(hkl) = \Omega/d(hkl)$, where Ω is the atomic volume. A large interplanar spacing therefore corresponds to a small planar unit cell and a consequently high planar atomic density. Consequently, the conclusion drawn from Figure 6 is that the densest planes in a given crystal structure, as well as their vicinal orientations of course, give rise to the lowest GB energies.[3,8,14]

A comparison with similar simulations for free surfaces[15] shows the disappearance of the minor cusps in Figure 6 along the edges and in the central regions of the triangle, leaving only those cusps associated with the three densest planes at the corners. Since free surfaces lack the three additional microscopic DOFs of GBs, this comparison illustrates the importance of translations at the interface in the minimization of the GB energy, particularly the energy of those boundaries with the smallest planar unit cells, which consequently give rise

to cusps (see Table I and Figure 6). By subtracting the GB energies in Figure 6 from those of free surfaces, γ, the ideal-cleavage energy associated with brittle decohesion at the GB, $2\gamma - E^{GB}$ (also known as the work of adhesion), is readily obtained. Without giving details, it is obvious from Figure 6 and the corresponding (much smoother) plot for free surfaces[15] that the GBs on the densest planes, as well as their vicinal orientations, also exhibit, by far, the highest cleavage energies.[14]

Finally, if the twist angle is now added as the third DOF (see Eq. 1), every point in the 2d phase space associated with the GB plane is unfolded into an infinite number of θ values, which, in Figure 5, are projected into a single point. The structure-energy plot for all symmetrical GBs may then be thought of as a 4d hypersurface. To gain some understanding of what this plot might look like, one can consider three-dimensional cross sections obtained as follows. By selecting a subset of planes perpendicular to a particular pole axis (for example, a ⟨110⟩ direction), a single tilt angle, Ψ, uniquely defines a given symmetrical GB plane.[4] If we now choose the twist angle as the second variable, a 3d cross section, $E^{GB}(\Psi\theta)$, of the 4d structure-energy hypersurface may therefore be obtained, which contains all symmetrical (tilt and twist) GBs with the same tilt axis.

One such cross section, perpendicular to ⟨110⟩, is shown in Figure 7.[14] The energies of the STGBs, appearing for twist angles of 180°, are the same as those in Figure 6 (see also Figure 5), while the variation of the GB energy as a function of θ is based on the extended Read-Shockley Eq. 4.[14] Figure 7 illustrates graphically that the STGBs are, indeed, a small — yet energetically favored — subset of twist boundaries. The cusped valleys in the figure demonstrate the importance of the densest lattice planes and their vicinal orientations. (For further details, as well as other cross sections, including the related ideal-cleavage energy, see Reference 14.)

Volume Expansion at GBs

The second aspect of the structure-energy correlation involves the microscopic DOFs. Rigid-body translations of the two halves of a bicrystal relative to each-other, $T = (T_x, T_y, T_z)$, can provide an important relaxation mechanism for minimizing the GB energy. When computing the relaxed atomic structure of a GB, a number of metastable translational configurations, with more or less equal energies, is often found to exist.

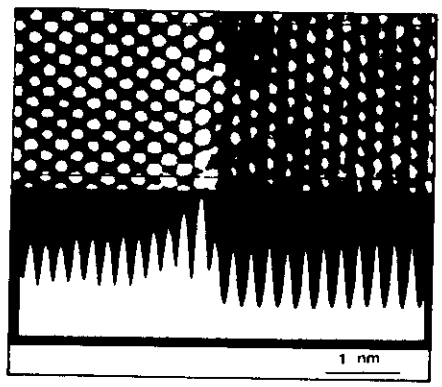

Figure 9. Digitized HREM image of an asymmetric (111)(001) tilt GB is analyzed for its volume expansion by utilizing an intensity scan across several (100) and (111) planes away from the GB region.

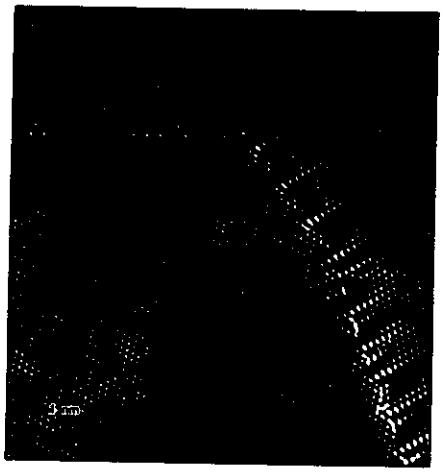

Figure 10. HREM image of symmetric and asymmetric GB configurations in Au with the same ⟨1$\bar{1}$0⟩, $\Psi \approx 50°$ (Σ11)[1] misorientation between the two grains (see also Figure 2b). A horizontal (113)(113) symmetric facet is followed by asymmetric (225)(441) and (557)(771) facets. Note the asymmetric lattice strains associated with both ATGBs.

For example, the short symmetric (221) segment shown in Figure 4, which has mirror symmetry, is not the preferred structure of the STGB on the (221) plane. This is evidenced by the existence of more extended facets of the same, but nonmirror-symmetric, GB found with different rigid-body translations parallel to the GB plane.[16] Not surprisingly, when the relaxed energies for two translational states are very close, multiple structures usually exist, a situation which experimentally manifests itself by the presence of localized steps separating well-defined facets.[16,17]

The z component of T should be particularly important from the point of view of the GB energy, because $T_z = \delta V$ accounts for a possible volume expansion per unit area at the GB and because volume is a thermodynamic variable. As pointed out more than 30 years ago, the volume expansion usually found at metallic GBs should thus be related directly to the energy (and electrical resistivity) of the boundary.[18] Recently, more extensive computer simulations, using various pair- and many-body potentials for fcc and bcc metals, have indeed confirmed the existence of a more or less linear relationship between the volume expansion per unit area and the related GB energy (see Figure 8). HREM observations of the volume expansion at the GB should thus provide a means for estimating its energy.

The HREM measurement of the volume expansion involves determining the positions of atomic columns or planes (if the latter are relatively dense) away from the boundary and comparing them to the unrelaxed GB structure. While different procedures can be employed (for details, see Reference 19), it is important to identify the GB core structure and GB plane. Figure 9 shows an example of a GB formed by two low-index planes, which permit the volume expansion to be determined through the analysis of the atomic-plane positions in this case. The volume expansion was also investigated for other ⟨110⟩ and ⟨100⟩ tilt GBs in Au;[16,20] these expansions are usually considerably larger, though, (typically by a factor of two) than the ones computed by means of the EAM potential for Au, indicating that such potentials may not be very well suited to describe the volume dependence of the GB energy. That the LJ-potential predictions agree much better with the experimental values is particularly surprising, since a local volume dependence of the interatomic interactions is taken into account explicitly only in the EAM potential.

Role of Atomic Matching Across the GB

The third aspect of the structure-energy correlation involves the role of the local atomic structure at the GB. Experimentally, a strong tendency for forming atomically well-matched regions at the interface, separated by highly localized

regions which accommodate the atomic level mismatch, is commonly observed[21] (see also Figure 10). This localized nature of atomic relaxations thus appears to favor structures that maintain, as much as possible, the coordination of the ideal lattice even at the interface.

A typical example is shown in Figure 10 for the STGB on the (113) plane and two asymmetrical facets with the same misorientation ($\Psi \approx 50°$; $\Sigma 11$). The regular arrangement of atomic columns in the symmetrical facet produces an optimum match between the two lattices, with no evidence of lattice strain. The greater length of the symmetrical configuration is due to its much lower energy, as compared with the two asymmetric facets in the figure (see also Figure 2b); the latter clearly exhibit extended regions of lattice strain. In some cases the tendency to minimize the number of broken bonds at the interface is so strong that a normally periodic GB instead forms a quasiperiodic — but better coordinated — structure with a lower energy.[16,21]

The role of the local coordination at the interface was also investigated by computer simulations. While for free surfaces a broken-bond description of the structure-energy correlation has been commonly used for more than half a century, such an approach has only recently been adopted for GBs. Figure 11 demonstrates the correlation between the average nearest-neighbor (nn) miscoordination, C, characterized by the number of broken nn bonds per unit area, and the GB energy. For comparison, the corresponding free-surface results are also shown.[15,22] While more distant neighbors should also play a role, in fcc metals their contribution was found to be rather small (typically about 10-20% of the nn contribution).

While the interface energy and C are reasonably well interrelated for both free surfaces and GBs (see Figure 11), the GB data scatter significantly. This scatter results from an intrinsic limitation of a broken-bond characterization of the atomic structure of GBs, largely because only the dislocation cores, and not their elastic strain fields, give rise to broken bonds.[22] A broken-bond description is therefore fully applicable only to high-angle GBs, which consist entirely of overlapping dislocation cores. In low-angle GBs, by contrast, an elastic (Read-Shockley[9]) contribution has to be added to the broken-bond (i.e., core) energy (see also Eq. 4). A more complete description of the atomic structure would involve the radial distribution function of the system, which also contains information on the elastic strain fields surrounding the GB dislocations.

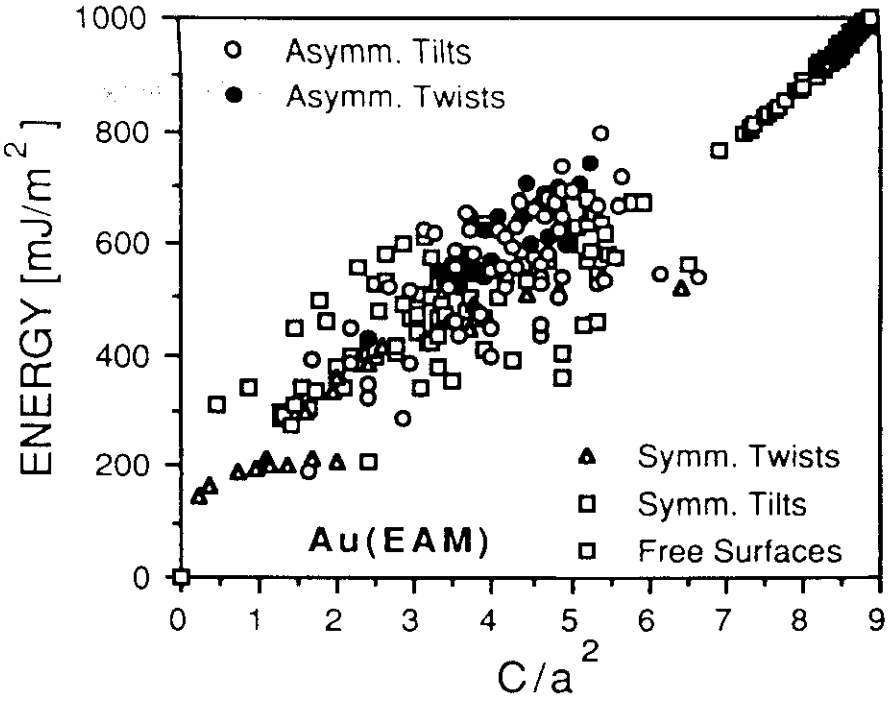

Figure 11. Correlation between GB energy (in mJ/m^2) and the number of broken nearest-neighbor bonds per unit area, C, for the EAM potential. For comparison, the related free-surface energies, γ, are shown also.[15,22] C is in units of a^{-2}.

The usefulness of any model for the atomic structure of solid interfaces should be assessed in terms of its ability to quantify the structure and thus permit a quantitative prediction of physical properties of GBs. The Read and Shockley[9] dislocation model provides an excellent example (see also Eq. 4). For nearly a quarter century, polyhedral-unit models have been used to describe the atomic structure of GBs in terms of the stacking of structural units along the GB plane.[23] However, the requirements of space filling at the interface and of the compatibility of the structural units with the adjoining grains generally cannot be satisfied simultaneously, unless the polyhedra are elastically distorted by strains that differ from one GB to another. Within the framework of these models, the atomic structure therefore has not been quantified. The above broken-bond characterization of the atomic structure of GBs represents, in essence, a quantified polyhedral-unit model, with its omission of elastic phenomena and hence its limitation to high-angle GBs in the Read-Shockley sense (in which the dislocation cores overlap completely).

Conclusions

We have attempted to illustrate how the complementary capabilities of HREM experiments and atomistic computer simulations can provide new insights into the correlation between the macroscopic, microscopic, and atomic structures of GBs and their energy.

An extensive exploration of the five-parameter misorientation phase space associated with the macroscopic DOFs is realistically possible only via simulation, while HREM experiments are limited to the tilt boundaries in this phase space. However, since the latter are fully governed by only the four DOFs associated with the GB plane, and because of their unique geometry, their HREM investigation provides valuable information on the role of the GB plane in their energy. In particular, the comparison of the relative lengths of symmetrical and asymmetrical facets provides semiquantitative information on their relative energies, while the detailed crystallographic analysis of such facets suggests a dominating role of the densest planes in the crystal lattice.

HREM experiments also provide valuable information on the three microscopic DOFs associated with rigid-body

translations at the GB. Extensive simulations, using both pair- and many-body potentials, demonstrate a practically linear relationship between the energy and volume expansion for GBs in metals (i.e., translations perpendicular to the GB plane). Translations parallel to the GB, by contrast, play a relatively minor role in the relaxed GB energy, although their optimization represents an important relaxation mechanism. Combined with the simulations, HREM measurements of the volume expansion thus provide direct information on the GB energy, while a comparison between measured and computed rigid-body translations parallel to the boundary provides an important test for (1) the validity of the interatomic potentials and (2) the relaxation procedures used in the simulations.

Finally, HREM experiments clearly demonstrate a tendency of the atomic structure to preserve a high degree of coherency across the interface. As in the case of free surfaces, the underlying causes, elucidated via simulation, are closely connected with the desire of the interface to minimize its number of broken bonds per unit area (i.e., its energy). However, such a broken-bond description of GBs ignores any elastic contribution to the GB energy, limiting its applicability to high-angle interfaces (in which the dislocation cores overlap completely). In all other interfaces both dislocation-core and strain-field phenomena may be of equal importance, and a Read-Shockley type of analysis based on Eq. 4 permits separation of the effects arising from the two distinct causes.

Acknowledgments

We gratefully acknowledge discussions with J. Jaszczak, S. Phillpot, and S. Yip. We also would like to thank L. Marks for making available the H9000 in the Department of Materials Science and Engineering at Northwestern University. This work was supported by the U.S. Department of Energy, BES Materials Sciences, under Contract No. W-31-109-Eng-38.

References

1. See, for example, C. Goux, *Can. Metall. Quarterly* **13** (1974) p. 9.
2. See, for example, W. Bollmann, *Crystal Defects and Crystalline Interfaces* (Springer Verlag, New York, 1970).
3. D. Wolf, *J. de Physique* **46** (1985) p. 197.
4. D. Wolf and J.F. Lutsko, *Z. Kristallographie* **189** (1989) p. 239.
5. D. Wolf, *Acta Metall.* **38** (1990) p. 781; ibid. p. 791.
6. M.S. Daw and M.I. Baskes, *Phys. Rev. B* **33** (1986) p. 7983.
7. R.W. Balluffi and R. Maurer, *Scripta Metall.* **22** (1988) p. 709.
8. D. Wolf and S.R. Phillpot, *Mater. Sci. Eng. A* **107** (1988) p. 3.
9. W.T. Read and Shockley, *Phys. Rev.* **78** (1950) p. 275.
10. D. Wolf, *Scripta Metall.* **23** (1989) p. 1713, ibid. 1913.
11. T. Schober and R.W. Balluffi, *Phil. Mag.* **21** (1970) p. 109.
12. T.Y. Tan, J.C.M. Hwang, P.J. Goodhew, and R.W. Balluffi, *Thin Solid Films* **33** (1976) p. 1.
13. K.L. Merkle, in *Proceedings of the 46th Annual Meeting of EMSA*, edited by G.W. Bailey (1988) p. 588.
14. D. Wolf, *J. Mater. Res.* MS #90-029, Vol. 5 #8, p. 1708.
15. D. Wolf, *Surf. Sci.* **226** (1990) p. 389.
16. K.L. Merkle, *Colloque de Phys.* **51 C1** (1990) p. 251.
17. K.L. Merkle and D.J. Smith, *Phys. Rev. Lett.* **59** (1987) p. 2887.
18. A. Seeger and G. Schottky, *Acta Metall.* **7** (1959) p. 495.
19. K.L. Merkle, *Scripta Metall.* **23** (1989) p. 1487.
20. F. Cosandey, S-W. Chan, and P. Stadelmann, *Colloque de Phys.* **51 C1** (1990) p. 109.
21. K.L. Merkle, in *Interfaces between Polymers, Metals, and Ceramics*, edited by B.M. DeKoven, A.J. Gellman, and R. Rosenberg (Mat. Res. Soc. Symp. Proc. **153**, Pittsburgh, PA, 1989) p. 83.
22. D. Wolf, *J. Appl. Phys.* (in press).
23. For a recent comprehensive review, see H. Gleiter, in *Atomistics of Fracture*, edited by R.M. Latanision and J.R. Pickens (Plenum, New York, 1983) p. 433. □